JOURNAL OF VIROLOGY, May 2006, p. 4326–4335 Vol. 80, No. 9
0022-538X/06/$08.00+0 doi:10.1128/JVI.80.9.4326–4335.2006

Enhanced Replication of Simian Immunodeficiency Virus Adjacent to Catecholaminergic Varicosities in Primate Lymph Nodes

Erica K. Sloan,[1] Ross P. Tarara,[2] John P. Capitanio,[2,3] and Steve W. Cole[1,4]*

Department of Medicine, Division of Hematology-Oncology, UCLA School of Medicine, UCLA AIDS Institute, and Cousins Center for Psychoneuroimmunology at the UCLA Semel Institute for Neuroscience and Human Behavior, Los Angeles, California[1]; California National Primate Research Center[2] and Department of Psychology,[3] University of California—Davis, Davis, California; and Jonsson Comprehensive Cancer Center and the UCLA Molecular Biology Institute, Los Angeles, California[4]

Received 24 August 2005/Accepted 25 January 2006

Clinical and in vitro studies have shown that activity of the autonomic nervous system (ANS) can stimulate lentivirus replication. To define the potential anatomical basis for this effect, we analyzed the spatial relationship between catecholaminergic neural fibers and sites of simian immunodeficiency virus (SIV) replication in lymph nodes from rhesus macaques experimentally infected with SIVmac251. Viral replication was mapped by in situ hybridization for SIV *env*, *gag*, and *nef* RNA, and catecholaminergic varicosities from the ANS were mapped by sucrose phosphate glyoxylic acid chemofluorescence. Spatial statistical analyses showed that the likelihood of active SIV replication increased by 3.9-fold in the vicinity of catecholaminergic varicosities ($P < 0.0001$). The densities of both ANS innervation and SIV replication differed across cortical, paracortical, and medullary regions of the lymph node, but analyses of each region separately continued to show increased replication of SIV adjacent to catecholaminergic varicosities. Ancillary analyses ruled out the possibility that SIV-induced alterations in lymph node architecture might create a spurious spatial association. These data support human clinical studies and in vitro molecular analyses showing that catecholamine neurotransmitters from the ANS can increase lentiviral replication by identifying a specific anatomic context for interactions between ANS neural fibers and replication of SIV in lymphoid tissue.

Clinical studies of human immunodeficiency virus type 1 (HIV-1) infection have documented accelerated clinical disease onset and an elevated plasma viral load among individuals subjected to long-term stress (6, 21), but the biological mechanisms mediating those effects have only recently begun to be explored. Laboratory-based clinical studies have identified activity of the autonomic nervous system (ANS) as a potential physiologic contributor to individual differences in HIV-1 pathogenesis (8, 10). Individuals with high levels of ANS activity show an increased HIV-1 plasma viral load and poorer suppression of viremia in response to antiretroviral therapy (10). In vitro studies show that the catecholamine neurotransmitters released by the ANS, epinephrine and norepinephrine, can accelerate HIV-1 replication via β-adrenergic activation of the cyclic AMP/protein kinase A (PKA) signaling pathway and subsequent increases in cell surface expression of viral coreceptors, enhancement of HIV-1 gene expression, and inhibition of antiviral cytokines (7, 9, 10). These results suggest that ANS activity could potentially modulate HIV-1 pathogenesis and, therefore, disease progression in vivo (8). However, the anatomic contexts that support interactions between ANS neurotransmitters and simian immunodeficiency virus (SIV)-replicating cells have not yet been defined.

The sympathetic branch of the ANS mediates "fight-or-flight" stress responses by secreting catecholamines into circulation and activating a network of neurons that target most organ systems of the body (31, 38). In addition to classical stress-responsive targets such as the cardiovascular, endocrine, and gastrointestinal systems, nerve fibers from the sympathetic nervous system also innervate all primary and secondary lymphoid organs (2, 23). Catecholaminergic neural fibers enter lymphoid organs in association with the vasculature and radiate out into parenchymal regions, particularly those populated by T lymphocytes and antigen-presenting cells (2). When activated by stress or other stimuli, micromolar quantities of norepinephrine are released from structural varicosities situated periodically over the length of the fibers (23, 32). Functional studies suggest that lymphoid tissue innervation may play a physiologic role in regulating immune responses by altering cellular activation, cytokine production, and effector cell generation (23). However, little is known about direct effects of neural activity on lymphotropic viruses. Given that HIV-1 replicates predominantly in lymphoid organs (12, 30), primate lentiviruses represent an opportune context for examining the effects of lymphoid innervation on viral pathogenesis.

We employed in situ hybridization and glyoxylic acid chemofluorescence to map the spatial relationship between catecholaminergic varicosites and SIV gene expression in lymph nodes biopsied from rhesus macaques at 37 weeks after infection with SIVmac251. The overarching aim of these studies is to determine whether SIV replication rates are altered in the vicinity of catecholaminergic varicosities, as would be expected based on previous clinical and in vitro studies of HIV-1 replication (7, 9, 10). We find a substantial increase in the density of SIV replication in T lymphocytes adjacent to catecholaminergic varicosities in vivo. This relationship also holds within distinct anatomic subcompartments of the lymph node, and

* Corresponding author. Mailing address: Department of Medicine, Division of Hematology-Oncology, 11-934 Factor Building, David Geffen School of Medicine at UCLA, Los Angeles, CA 90095-1678. Phone: (310) 267-4243. Fax: (310) 794-9247. E-mail: coles@ucla.edu.

comparisons with tissues from uninfected animals show that such effects cannot be explained by SIV-induced changes in lymph node architecture or innervation density. These data suggest that ANS activity within the primate lymph node might significantly promote lentiviral replication in vivo.

MATERIALS AND METHODS

Subjects. These studies examined lymph nodes biopsied from adult male rhesus macaques born into half-acre outdoor enclosures at the California National Primate Research Center and reared in their natal groups of 80 to 120 animals. Animals were relocated to individual indoor cages approximately 22 months prior to inoculation, and the mean age at inoculation was 8.7 years (range, 7.2 to 10.3 years). After immobilization with ketamine hydrochloride (10 mg/kg), animals were inoculated intravenously with $10^{2.66}$ 50% tissue culture infective doses of SIVmac251 (grown in rhesus peripheral blood mononuclear cells and titered by infection of CEMx174 cells) or an equivalent volume of saline. At 37 weeks postinfection, lymph nodes were biopsied, as described below, from 20 animals remaining alive at that time point. All procedures were carried out under protocols approved by the Institutional Animal Use and Care and University Institutional Review Boards at the University of California's Davis and Los Angeles campuses.

Viral load and CD4$^+$-T-cell counts. Blood was collected from nonanesthetized animals at 1500 to 1530 h using nonheparinized syringes and immediately transferred to a tube containing EDTA. Complete blood counts were performed using a Serono Baker diagnostic system (Allentown, PA), and all electronic counts were verified by a manual differential. Flow cytometry was used to phenotype lymphocyte subsets. Whole blood was incubated with phycoerythrin-anti-CD4 (clone M-T477), peridinin chlorophyll protein-anti-CD8 (clone SK1), and fluorescein isothiocyanate-anti-CD3 (clone SP34) (all antibodies from BD Pharmingen). Red cells were lysed, the samples were fixed using Coulter Q-prep (Coulter Corp.), and lymphocytes were gated by forward- and side-light scatter using a FACSCalibur flow cytometer (BD Pharmingen). SIV RNA was quantitated using an SIV-specific branched-DNA signal amplification assay as described previously (22).

Lymph nodes. Animals were immobilized with ketamine hydrochloride (10 mg/kg) and metatomidine (0.03 mg/kg) intramuscularly, and a subcutaneous injection of bupivicaine was administered proximal and medial to the biopsy site. Lymph nodes were biopsied from 20 monkeys (9 control and 11 SIV-positive [SIV$^+$] monkeys) that were alive at 37 weeks postinoculation. Four axillary lymph nodes were removed from each animal and frozen in liquid nitrogen. A random sample of 9 lymph nodes from six saline-injected control monkeys and 13 lymph nodes from nine SIVmac251-infected animals were sectioned at 16 μm by cryostat in a randomly selected orientation, and adjacent sections were (i) stained by hematoxylin and eosin (H&E) for general morphology, (ii) assayed by in situ hybridization for SIV replication as described below, and (iii) assayed by sucrose-phosphate-glyoxylic acid (SPG) histofluorescence for catecholamine-containing neural fibers, as detailed below.

In situ hybridization. Sites of active SIV replication were mapped by in situ hybridization using probes to detect SIV *env*, *gag*, and *nef* mRNA. Frozen sections were fixed in 4% paraformaldehyde, digested in 1 mg/ml proteinase K (Sigma) for 5 min at 37°C, and prehybridized in hybridization buffer (50% formamide, 10% dextran sulfate, 0.05% sodium dodecyl sulfate, 0.05% polyvinylpyrrolidone, 500 μg/ml boiled salmon sperm DNA, 260 μg/ml *Saccharomyces cerevisiae* tRNA, 50 mM Tris HCl, pH 7.4, 300 mM NaCl, 2 mM EDTA) for 2 h at 37°C. Single-stranded DNA probes were synthesized by PCR and labeled with digoxigenin (Boehringer Mannheim) as previously described (4). A cocktail of all three complementary probes (or three sense probes as a negative control) were mixed in hybridization buffer, denatured at 65°C for 5 min, and hybridized to the sections at 37°C overnight. After hybridization, slides were washed successively at 37°C in 2× SSC (1× SSC is 0.15 M NaCl plus 0.015 M sodium citrate), 1× SSC, and phosphate-buffered saline before incubation at 25°C for 30 min in DIG detection kit blocking solution (Boehringer Mannheim). Hybridization was visualized using an alkaline phosphatase-conjugated anti-digoxigenin antibody (Boehringer Mannheim) incubated in NBT/X-phosphate (Boehringer Mannheim) solution for 4 to 6 h. Sections were counterstained in neutral red or costained by immunofluorescence and were coverslipped with aqueous mounting medium.

Immunofluorescence. Paraformaldehyde-postfixed sections were pretreated with avidin and biotin solutions (DakoCytomation) to block endogenous biotin and incubated overnight at 4°C with primary antibodies against CD3 (rabbit polyclonal; DakoCytomation), CD20 (L26; Zymed), macrophage marker (HAM56; DakoCytomation), follicular dendritic cell marker (CNA.42; DakoCytomation), CXCR4 (12G5; BD Biosciences), CCR5 (3A9; BD Biosciences), or negative control mouse immunoglobulin G or immunoglobulin M (DakoCytomation). Sections were washed and incubated with the appropriate Alexa-conjugated secondary antibody (Molecular Probes) or biotinylated secondary antibody (Vector Laboratories) followed by streptavidin-Alexa (Molecular Probes). Sections were counterstained with Hoechst 33342 (Molecular Probes), coverslipped, and imaged by fluorescence microscopy. In some cases, staining with in situ hybridization appeared to block subsequent binding of antibodies, preventing conclusive identification of SIV$^+$ cells. However, all SIV$^+$ cells showed small circular lymphocyte-like morphology, suggesting a minimal contribution to the SIV RNA signal from follicular dendritic cells.

Catecholamine fluorescence. Spatial distribution of catecholaminergic nerve fibers was mapped by SPG chemofluorescence (11) with an established counterstaining modification (15). Briefly, 16-μm frozen sections were melted onto glass slides and dipped immediately in glyoxylic acid-malachite green solution (1% glyoxylic acid, 0.236 M monobasic KH_2PO_4, 0.2 M sucrose, 1.75 mg/ml malachite green, pH 7.4) for 5 s and then dipped into glyoxlic acid solution without malachite green for 5 s. Slides were dried completely under a stream of cool air and then covered by a drop of light mineral oil and heated to 95°C for 2.5 min. Slides were cooled and coverslipped. Blue-white catecholamine fluorescence was quantified by fluorescence microscopy using a long-pass UV filter (Chroma Technologies) as described below.

Image processing. For analysis of in situ hybridization/immunofluorescence coexpression, SIV$^+$ cells were detected by in situ hybridization for SIV-specific transcripts using NBT/X-phosphate chromogen and imaged by bright-field microscopy. The same field was imaged by multichannel fluorescence microscopy for antibody staining of cell surface markers (CD3/CD20 or HAM56/CD20) and Hoechst 33342 nuclear stain. Bright-field images were inverted and overlaid with fluorescence images using Photoshop 7.0 to show colocalization of SIV$^+$ cells and cell surface markers. Similar multichannel fluorescence imaging of a single field and image overlay was also used to identify cells permissive for viral infection using cell surface markers (CD3/CD4 or CD3/CCR5). For analysis of the relationship between catecholaminergic innervation and sites of SIV replication, each lymph node section was digitally imaged over its entire surface at ×200 magnification using an Axioskop 2 microscope (Zeiss). Images were acquired with an AxioCam HRc color camera and AxioVision 4.1 software (Zeiss). Individual images were assembled to compose a single digital file representing the entire section, and a grid of 250-μm^2 spatial units was superimposed to provide registration between adjacent tissue sections (as illustrated in Fig. 5a). Anatomic subregions of each lymph node (cortex, paracortex, and medulla) were identified in H&E-stained sections by an experienced veterinary pathologist (R.P.T.) blind to data on the location of catecholaminergic neural fibers and SIV RNA. Each spatial grid unit or "quadrat" was assigned to a single anatomic subregion, and quadrats spanning two or more anatomic subregions were divided to ensure that each analyzed unit represented a single anatomic region. The density of mononuclear cells within quadrats from the cortex, paracortex, and medulla was measured by cell counts of H&E-stained sections from five lymph nodes from SIV$^+$ animals and five lymph nodes from uninfected controls. Cells were counted in three randomly selected quadrats from each anatomical region in each node while the pathologist was blinded to the conditions.

We used an unbiased stereologic approach to estimate the density of SIV replication sites in lymph node tissue quadrats that contained one or more catecholaminergic varicosities versus quadrats that contained none. Using the approach described previously by Mouton (26), we (i) sectioned lymph nodes in randomly selected orientations to provide a random two-dimensional (2-D) sample through three-dimensional (3-D) tissue space, (ii) enumerated SIV replication sites and catecholaminergic varicosities in all 2-D tissue quadrats within each section, (iii) used the Delesse area-volume principle (26) to estimate the 3-D density of SIV replication from 2-D SIV RNA frequency data in tissue units with catecholaminergic varicosities versus those without catecholaminergic varicosities, and (iv) carried out all statistical comparisons using an intranode approach (i.e., producing a tissue-specific estimate of differential SIV replication density in quadrats containing one or more catecholaminergic varicosities compared to quadrats containing none for each tissue sample and then averaging estimates of that difference across multiple tissue samples to generate a population level estimate from our randomly sampled tissues). This approach permits an accurate estimation of 3-D SIV replication density from 2-D histological profiles while controlling for technical sources of bias (e.g., differential tissue shrinkage across nodes, differences in lymph node size, variations in the distribution of subregions such as cortex, paracortex, and medulla, etc.) (26). Using this approach, any errors in estimating the number of catecholaminergic varicosities in each tissue quadrat will lead to a conservative underestimate of the

true difference in SIV replication rates in tissues that do contain ANS innervation compared to those that do not contain ANS innervation (25).

Data analysis. The spatial association between ANS neural fibers and sites of SIV replication was measured by the Cochran-Mantel-Haenszel χ^2 analysis (14), which relates the frequency of SIV replication sites to the number of fluorescent SPG varicosities in each spatial quadrat within a given lymph node. Results for each individual lymph node were then averaged together to provide an aggregate measure of association across all lymph nodes analyzed (14). In addition to basic analyses aggregating over an entire lymph node, we also separately analyzed the spatial units from the cortical, paracortical, and medullary regions to control for potential differences across anatomic regions. In these analyses, measures of spatial association were computed over units from a single anatomic region, and the resulting measures were averaged across comparable regions from each specimen to provide an aggregate analysis of association.

To determine whether SIV infection might influence lymph node innervation, we also carried out χ^2 analyses to compare the density of catecholaminergic neural fibers in lymph nodes (or anatomic subregions of lymph nodes) from SIV-infected animals to the density of those from control animals. The frequency of SIV replication sites varied substantially across lymph nodes from SIV-inoculated animals, and Spearman correlations were computed to determine whether an increasing prevalence of SIV replication within a given lymph node might relate to the prevalence of catecholaminergic varicosities.

RESULTS

To assess the level of SIV replication in the vicinity of catecholaminergic neural fibers in vivo, we assayed 22 lymph nodes biopsied from 15 rhesus macaques 37 weeks after inoculation with SIVmac251 or a vehicle control. Viral loads and $CD4^+$-T-cell counts at the time of biopsy are shown in Table 1. The average survival time of SIV-infected monkeys was 462 days (range, 268 to 713 days) (Table 1), and tissue sampling at 37 weeks ensured that animals were in mid-stage chronic infection at the time of analysis. Routine pathological studies found that lymph nodes from SIV-infected animals were generally in an unreactive or resting state with an unexpanded paracortex and no (in 10 of 13) or few (in 3 of 13) cortical secondary follicles. Sinuses showed slight cellularity (lymphocytes and histiocytes), with no plasma cells in the medullary cords. Host cells permissive for SIV infection were present throughout the paracortex, cortex, and medullary regions, as evidenced by CD4 and CCR5 immunoreactivity in these regions (Fig. 1). $CCR5^+$ T cells were present within the paracortex, particularly at the interface with germinal centers, in the medullary regions, and within the interfollicular regions of the cortex.

Catecholaminergic innervation of rhesus macaque lymph nodes. To determine the location of functional ANS neural fibers within the primate lymph node, we used SPG chemofluorescence to map the distribution of catecholamine-containing nerve fibers. Catecholaminergic fibers were detected in the parenchyma of 23 of the 24 lymph nodes analyzed, including all specimens from uninfected controls. Figure 2 shows an example of SPG mapping of catecholaminergic neural fibers in an axillary lymph node. As previously found in rodent samples (2), macaque lymph nodes show frequent dense innervation surrounding blood vessels (Fig. 2a) and branching innervation of the lymph node parenchyma (Fig. 2b). Parenchymal innervation is marked by dendritic structures bearing frequent varicosities that are believed to represent sites of neurotransmitter release (16) (marked by arrows in Fig. 2b). SPG chemofluorescence is specific to catecholamine neurotransmitters, so these findings confirm previously reported indications that mammalian lymphoid tissues show parenchymal innervation by the sympathetic division of the ANS (i.e., catecholaminergic nerve fibers not associated with vasculature) (23, 34, 37). These results show that primate lymph nodes maintain ANS neural fibers bearing catecholamine neurotransmitters that could potentially influence lentiviral replication.

TABLE 1. Plasma viral load, $CD4^+$-T-lymphocyte count, and postinfection survival times for rhesus macaques infected with SIVmac251

Animal	Viral load (RNA copies/ml [10^6])	$CD4^+$ T lymphocytes (cells/mm^3)	Survival (days postinfection)
1	0.21	594	519
2	0.41	242	713
3	0.64	244	604
4	0.96	181	406
5	2.80	80	393
6	3.40	371	468
7	6.05	689	460
8	6.48	432	330
9	10.90	205	268

SIV replication. Figure 3 (a to d) shows in situ hybridization to detect SIV RNA from the *gag*, *pol*, and *nef* genes in a lymph node from an SIV-infected animal. Parallel analyses with uninfected lymph nodes or sense-strand probes on infected lymph nodes were consistently negative (Fig. 3e and f), demonstrating specific detection of sense-strand SIV RNA by this assay. To determine which cell types supported SIV replication in the tissues studied, we costained tissue sections for CD3 (T lymphocytes) and CD20 (B lymphocytes) or the macrophage marker HAM56 and CD20. Viral replication in macrophages and B cells has previously been described for another strain of SIV (27) and for HIV-1 (28), but other groups have found replicating HIV-1 infection only in $CD45RO^+$ memory T cells (35). Simultaneous analysis by in situ hybridization and immunofluorescence for cell surface markers showed that $CD3^+$ T lymphocytes represented the majority of SIV-infected cells in our samples (Fig. 4). Macrophages containing detectable SIV RNA were rare but occasionally present (Fig. 4), particularly at the interface with germinal centers. Costaining with a follicular dendritic cell (FDC)-specific antibody showed that the FDC network was intact in lymph node germinal centers (data not shown). However, virions trapped in the FDC network did not contain sufficient SIV RNA to be detectable by our in situ hybridization probes (data not shown), despite predigestion with proteinase K (35).

Spatial relationship between catecholaminergic neural fibers and SIV replication. To assess the relationship between ANS neural fibers and sites of active SIV replication, we compared the frequency of SIV replication in lymph node tissue adjacent to parenchymal catecholaminergic varicosities with replication at sites distant from varicosities. To facilitate a quantitative analysis, each lymph node section was divided into 250-μm^2 spatial quadrats (Fig. 5a), and the number of SIV replication sites in quadrats containing one or more parenchymal catecholaminergic varicosities (i.e., ANS neural fibers not associated with blood vessels) was compared with the number of SIV replication sites in quadrats containing no parenchymal varicosities. Across all specimens analyzed, an average of 0.179 SIV replication sites were observed in tissue quadrats containing no varicosities, and an average of 0.275 replication sites

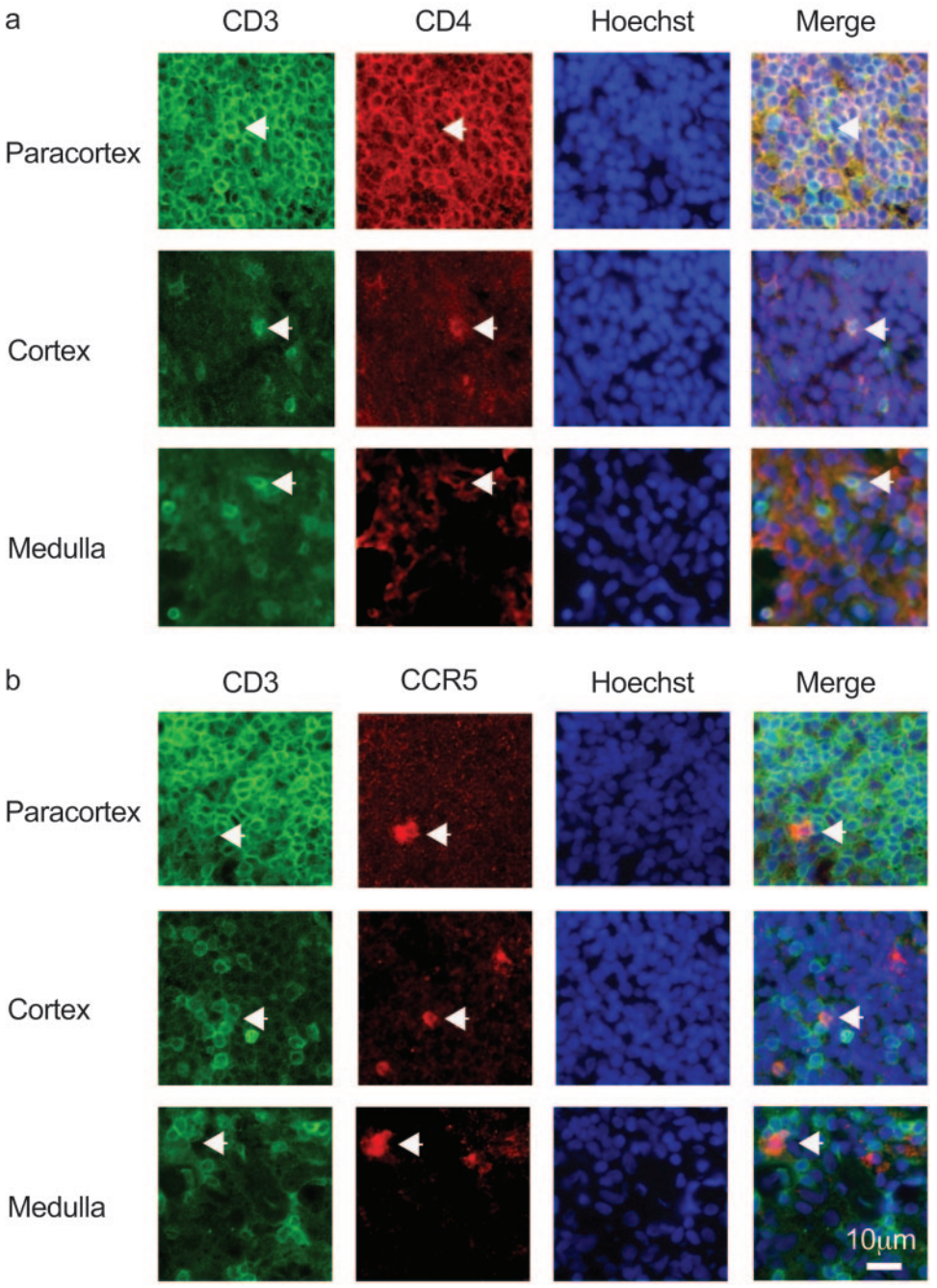

FIG. 1. Cells permissive for SIV infection in lymph node subregions. Eight-micrometer lymph node sections were incubated with primary antibodies against CD3 to identify T cells (a and b) and CD4 (a) or CCR5 (b) to identify virus-permissive host cells, followed by incubation with fluorescence-conjugated secondary antibodies and the nuclear stain Hoechst 33342. Each field was imaged by multichannel fluorescence microscopy, and images were overlaid (Merge) to show the presence of $CD3^+/CD4^+$ cells (a, white arrowheads) or $CD3^+/CCR5^+$ cells (b, white arrowheads) in the paracortex, cortex, and medullary regions.

were observed in quadrats containing one or more parenchymal varicosities ($P = 0.0042$ by t test). Similar results emerged when tissue quadrats were classified as showing one or more SIV replication sites versus no replication sites, with the odds of active SIV replication increasing by 3.9-fold in quadrats containing catecholaminergic varicosities (χ^2 [1] = 53.39; $P < 0.0001$) (Fig. 5c). Figure 5d shows the distribution of SIV replication sites in representative medullary quadrats showing one or more parenchymal varicosities versus no parenchymal varicosities. Analysis of the absolute number of catecholaminergic varicosities and SIV replication sites in each quadrat also revealed a positive linear correlation, with the number of SIV replication sites increasing by an average of 0.015 with each additional varicosity present (analyzed by linear regression; $P < 0.0001$). Thus, several alternative analyses converge to show that SIV replicates at an increased frequency in the

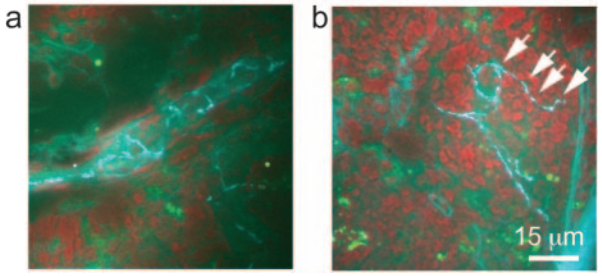

FIG. 2. Detection of sympathetic neurons by SPG fluorescence. Sixteen-micrometer lymph node sections were stained by SPG for chemofluorescence detection of catacholaminergic varicosities. Catecholaminergic innervation was present around blood vessels (a), throughout the paracortical parenchyma (b), and through parenchymal regions of the cortex and medulla (data not shown). Arrows indicate catecholaminergic varicosities believed to represent primary sites of catecholamine release (16).

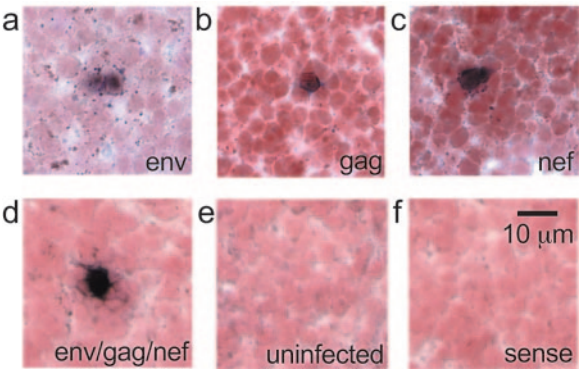

FIG. 3. Detection of SIV replication by in situ hybridization. Digoxigenin-labeled probes for SIV *env*, *gag*, and *nef* mRNA were hybridized to 16-μm lymph node sections from SIV-infected animals (a to c). A cocktail of all three antisense probes was used to map sites of active SIV replication (d). Assay specificity was verified by the absence of antisense probe binding to tissue from uninfected controls (e) and by the absence of sense probe binding to SIV-infected tissue (f).

vicinity of parenchymal catecholaminergic varicosities within secondary lymphoid tissues.

One of the animals studied (Table 1, animal 9) showed a high viral load in plasma and low CD4 counts at the time of lymph node biopsy and was euthanized 10 days later. To ensure that data from this animal did not bias results observed for other animals during mid-stage infection, spatial association analyses were repeated after animal 9 was excluded. Similar results emerged, with significantly higher odds of active SIV replication in tissue quadrats containing one or more parenchymal varicosities versus no parenchymal varicosities (odds ratio = 2.60; χ^2 [1] = 15.65; $P < 0.0001$). Similar results also emerged after three lymph node specimens showing mild cortical expansion were excluded (odds ratio = 4.31; χ^2 [1] = 64.99; $P < 0.0001$). Thus, the effects of individual variation on disease progression and lymph node architecture did not account for the observed relationship between parenchymal varicosities and SIV replication.

SIV-ANS interaction across anatomic subregions. The densities of both SIV replication and catecholaminergic varicosities differed significantly across anatomic subregions of the lymph node (Fig. 6). Across all SIV^+ samples surveyed, viral gene expression was detected in 11.4% of cortical quadrats, 20.7% of paracortical quadrats, and 12.9% of medullary quadrats (Fig. 6) (difference across regions, χ^2 [2] = 40.99 and $P < 0.0001$). The density of catecholaminergic varicosities showed a parallel variation across subregions, with one or more parenchymal varicosities observed in 4.1% of cortical quadrats, 12.3% of paracortical quadrats, and 11.2% of medullary quadrats (Fig. 6) (difference across regions, χ^2 [2] = 94.01 and $P < 0.0001$). To ensure that the tissue-wide association between catecholaminergic varicosities and SIV replication sites did not stem solely from their cosegregation within distinct anatomic subcompartments, we repeated spatial association analyses within each subregion separately. The odds of SIV replication were 4.04-fold higher in cortical quadrats containing one or more varicosity (χ^2 [1] = 27.33; $P < 0.0001$) and 5.46-fold higher in medullary quadrats containing one or more varicosity (χ^2 [1] = 9.89; $P < 0.0017$). The odds of SIV replication were 1.32-fold higher in paracortical quadrats containing one or more catecholaminergic varicosities than in quadrats containing none, but that difference did not reach statistical significance. Spatial association analyses that controlled for differences across anatomic subregions continued to find that the odds of active SIV replication were 3.1-fold higher in tissue units containing one or more catecholaminergic varicosities than those that contained none (χ^2 [1] = 29.83; $P < 0.0001$). Thus, elevated SIV replication in the vicinity of catecholaminergic varicosities is not an artifact of the two variables' cosegregation within distinct anatomic subcompartments of the lymph node, and a significant spatial association is observed even within individual subcompartments.

Effects of SIV replication on innervation density. Higher levels of SIV replication in the vicinity of catecholaminergic neural fibers is consistent with in vitro studies showing that catecholamines can accelerate HIV-1 replication (7, 9). An alternative explanation for spatial association is that SIV infection might enhance the expression or maintenance of neural fibers (e.g., via production of growth factors by activated leukocytes). To evaluate this possibility, we compared the density of parenchymal catecholaminergic varicosities in lymph nodes from uninfected control animals with that observed in lymph nodes from SIV-infected animals. Lymph nodes from SIV-infected animals showed a significantly lower density of parenchymal varicosities across the organ as a whole and across distinct anatomic subregions (Fig. 7). Lymph nodes from SIV-infected animals showed levels of catecholaminergic varicosities similar to those of uninfected controls in the cortex, but medullary innervation was marginally reduced (difference from uninfected, χ^2 [1] = 3.56 and $P = 0.059$), and paracortical innervation was significantly reduced (difference from uninfected, χ^2 [1] = 20.95 and $P < 0.0001$). As a result of reduced medullary and paracortical innervation, lymph nodes from SIV-infected macaques showed a 41% lower density of catecholaminergic varicosities compared to uninfected controls (mean, 1.32 parenchymal varicosities per quadrat in uninfected controls versus 0.54 parenchymal varicosities in SIV-infected specimens; $P < 0.0001$ by t test). These findings are inconsistent with the hypothesis that relationships between parenchymal varicosities and SIV gene expression stem from virus-induced enhancement of varicosity density.

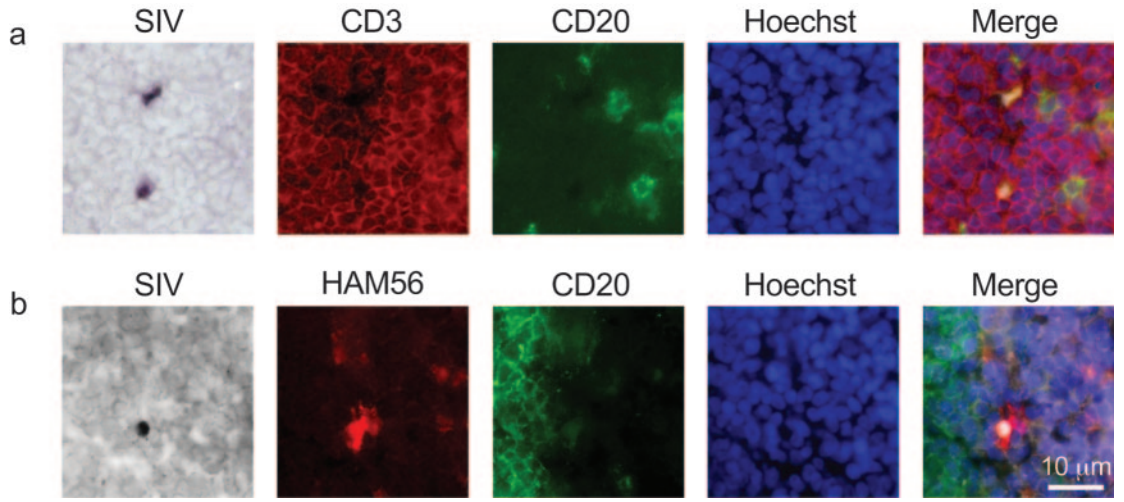

FIG. 4. Phenotype of SIV$^+$ cells in macaque lymph nodes. SIV$^+$ cells were identified in lymph node sections by in situ hybridization and imaged by bright-field microscopy (two separate fields shown in a and b). Each field was imaged in parallel by fluorescence microcopy to detect the T-cell marker CD3 (a), the macrophage marker HAM56 (b), the B-cell marker CD20 (both a and b), and the nuclear stain Hoechst 33342. To create the merged image, each bright-field image (a and b) was inverted so that SIV$^+$ cells appear white and overlaid with fluorescence images to show colocalization of SIV$^+$ mRNA and cell surface antigens.

To confirm that SIV replication was not associated with catecholaminergic varicosities as a consequence of virally mediated enhancement of local innervation, we approached this question in a second way by assessing the variation in the innervation of lymph nodes from SIV-infected animals that differed in the number of SIV replication sites present. Consistent with the results reported above, lymph nodes with a higher density of SIV replication showed a tendency toward a lower density of catecholaminergic varicosities, although this relationship did not reach statistical significance (Spearman $r = -0.42$; $P = 0.174$). Such results are not consistent with the hypothesis that SIV replication produces a local increase in the density of neural fibers.

We also sought to determine whether SIV infection might alter cell densities within the lymph node tissue and thus potentially alter the relationship between SIV-infected cells and parenchymal varicosities. In randomly sampled quadrats of the cortex, paracortex, and medulla, analysis of cell numbers showed a density of mononuclear cells in tissues from SIV-infected animals that was comparable to that in tissues from uninfected controls. Mean cell counts per 250-μm^2 spatial quadrat were 604 in the medulla of SIV$^+$ tissues compared to 539 in uninfected controls (difference, $P = 0.382$), 589 compared to 542 in the cortex (difference, $P = 0.293$), and 600 compared to 550 in the paracortex (difference, $P = 0.239$). These results are consistent with the histopathological analyses described above, confirming that lymph nodes were sampled during mid-stage infection and did not show any significant lymphopenia that might distort the relationship between ANS neural fibers and sites of SIV gene expression.

DISCUSSION

The present studies identify a neuroanatomic context in which ANS activity can interact with SIV-infected cells to facilitate lentiviral replication in vivo. In experimentally infected rhesus macaques, levels of active SIV replication were significantly higher in the vicinity of catecholaminergic neural fibers within the lymph node parenchyma. Compared to regions containing no catecholaminergic innervation, the odds of SIV replication were approximately fourfold higher in lymph node tissue units containing one or more parenchymal catecholaminergic varicosities. This relationship held at the level of the lymph node as a whole and within distinct anatomic subregions (medulla and cortex). Such results are consistent with the hypothesis that norepinephrine released from ANS neural fibers might enhance viral load in HIV-1 patients (10) and with in vitro studies defining specific molecular mechanisms by which norepinephrine can accelerate HIV-1 replication (7, 9, 10). The present data extend those findings to identify a specific anatomic nexus in which ANS signaling can interact with virally infected cells to influence the lentiviral replication cycle in vivo. In addition to providing a lymphoid tissue context for catecholamine effects on viral replication, these findings also suggest that adrenergic interventions aimed at blocking such interactions must be capable of penetrating into secondary lymphoid organs to be effective.

The most parsimonious explanation of the spatial association between ANS neural fibers and SIV replication is that catecholamines can accelerate SIV replication via the same molecular mechanisms previously identified for HIV-1 in vitro (7, 9, 10). However, other mechanisms could potentially contribute to spatial association. For example, catecholamine-induced signaling through the PKA pathway is known to inhibit cytotoxic T-cell activity (17, 18, 36). This could impair cellular immunity in the vicinity of catecholaminergic varicosities and thus extend the duration of productive viral gene expression. It is also possible that catecholamines might selectively recruit or retain cells already supporting SIV replication via PKA-mediated effects on chemokine receptors or adhesion molecules (3, 7, 10, 29). Although theoretically possible, no previous studies have demonstrated chemotactic attraction of activated or virally infected leukocytes to catecholaminergic nerve fibers. An-

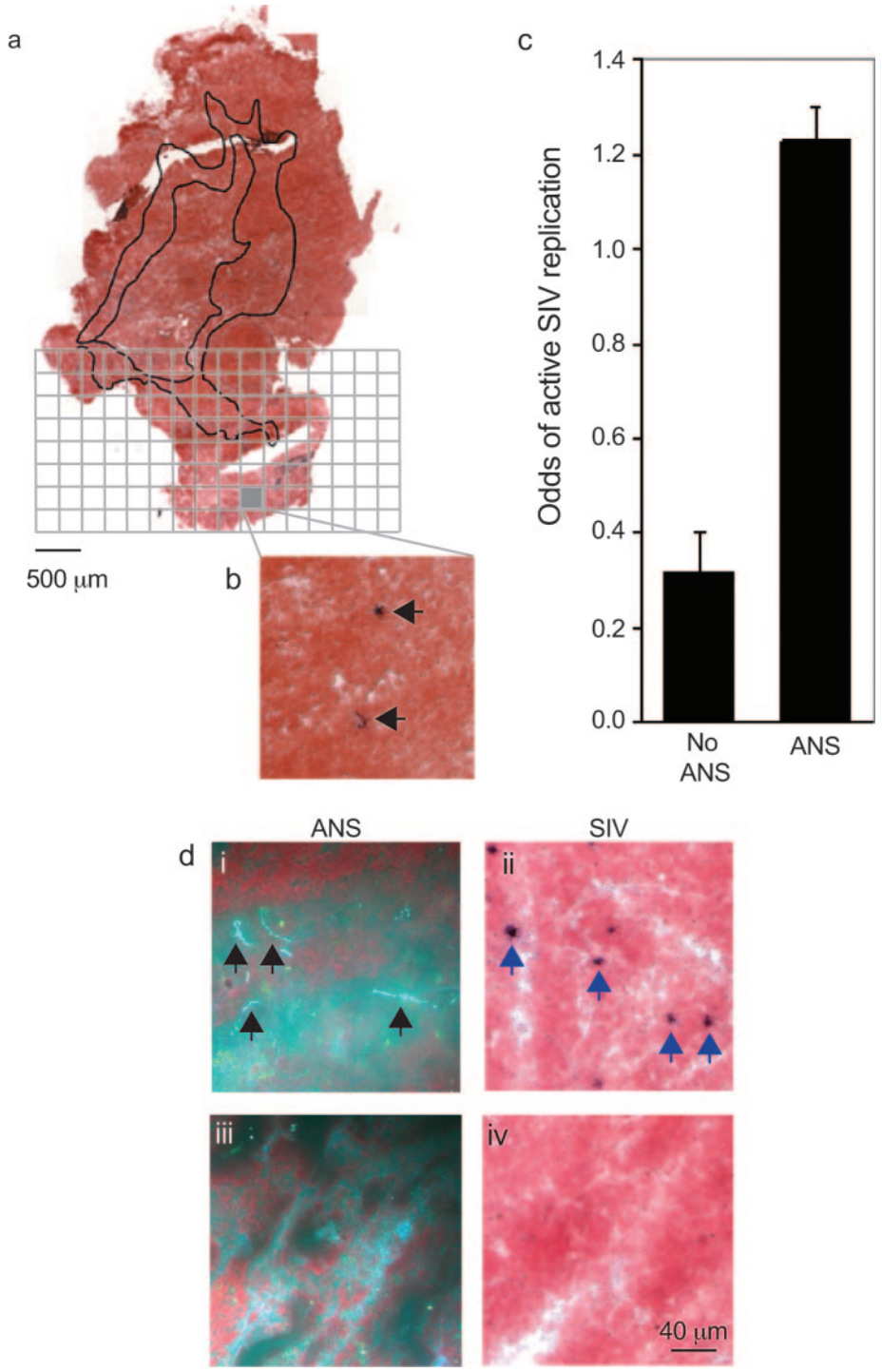

FIG. 5. Colocalization of SIV replication and ANS innervation. Spatial frequency of SIV replication throughout the entire lymph node section (a) was defined by the number of active viral replication foci (arrowheads) in 250-μm^2 spatial units or quadrats (b). (c) Odds of active SIV replication (by in situ hybridization) in 250-μm^2 quadrats that contain one or more parenchymal catecholaminergic varicosities (ANS) versus none (no ANS). Statistical significance of the differential frequency across the total 4,300 assessed quadrats was analyzed by Cochran-Mantel-Haenszel χ^2 analysis (odds ratio = 3.9; difference, $P < 0.0001$). (d) Representative quadrats from adjacent 16-μm sections, with catecholaminergic varicosities mapped by SPG chemofluorescence (black) and SIV replication mapped by in situ hybridization for viral RNA (blue arrowheads). (i and ii) Representative example of lymph node medulla with active SIV replication (ii) in the vicinity of catecholaminergic varicosities (i). (iii and iv) Representative example of lymph node medulla showing no SIV replication (iv) in a quadrat lacking catecholaminergic varicosities (iii).

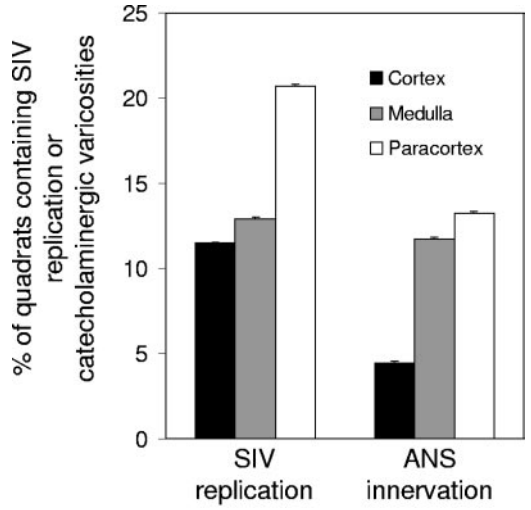

FIG. 6. Distribution of SIV replication and ANS innervation across anatomic subcompartments. Densities of innervation and SIV replication were quantified as the percentage of tissue quadrats from cortex, paracortex, or medulla showing one or more SIV replication foci or one or more catecholaminergic varicosities in parenchymal tissue (i.e., excluding blood vessel-associated neural fibers), respectively. Error bars equal standard errors of the means.

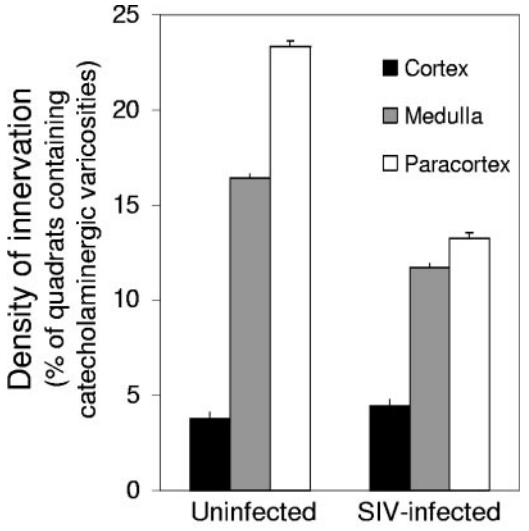

FIG. 7. Density of sympathetic innervation across anatomical subregions of lymph nodes from uninfected and SIV-infected macaques. Innervation was mapped by SPG chemofluorescence, and data represent the percentages of 250-μm^2 quadrats containing catecholaminergic varicosities within cortex (black), medulla (gray), and paracortex (white) in 13 lymph nodes from SIV-infected animals and 9 lymph nodes from uninfected animals. Error bars equal standard errors of the means.

other potential mechanism for colocalization is the selective recruitment of catecholaminergic fibers by cellular processes associated with SIV replication. Activated leukocytes produce neurotropic factors and cytokines that could support the growth or maintenance of neural fibers (1, 19). This hypothesis might account for the localized association between catecholaminergic varicosities and SIV replication within a given lymph node, but it is not consistent with the strong inverse relationship observed between SIV replication frequencies and overall innervation density across different lymph nodes. In comparisons among SIV-infected tissues with different levels of viral replication, and in comparisons between SIV-infected and -uninfected tissues, higher rates of SIV replication were consistently associated with a lower density of catecholaminergic varicosities. Thus, the spatial colocalization observed within a given lymph node is not likely to be mediated by SIV-induced enhancement of local innervation. Another possibility is that changes in lymph node architecture induced by SIV pathogenesis could act to cosegregate SIV-expressing cells in the same vicinity as catecholaminergic neural fibers (e.g., by selectively decreasing the size of anatomic subcompartments, such as the paracortex, that contain high levels of both catecholaminergic nerve fibers and SIV replication). However, statistical analyses that controlled for differential distribution of SIV-expressing cells and parenchymal catecholaminergic varicosities across anatomic subregions continued to show a strong spatial relationship between those two parameters within structurally homogenous anatomic subcompartments. Moreover, the use of a stereologically based density estimate (SIV-expressing cells per 250-μm^2 tissue unit) ensured that changes in the overall cellularity or size of the lymph node cannot account for the relationships observed (see reference 26 for more detail on statistical control for stereological bias). Finally, empirical analysis of cellularity showed that the mid-stage SIV infection analyzed here was not associated with any significant decrease in cell density that might act to cosegregate ANS neural fibers and SIV-replicating cells (in fact, a slight and nonsignificant increase in cell density was noted). These results show that SIV gene expression is selectively increased in the vicinity of catecholaminergic varicosities within the lymph node parenchyma and that such relationships are independent of any overall change in innervation or SIV gene expression that might result from global changes in lymph node structure or cellularity. Given the lack of empirical support for alternative explanations, catecholamine-induced stimulation of viral replication represents the best-substantiated explanation for the colocalization observed in these studies. However, future studies involving experimental manipulation of such interactions will be required to definitively identify the mechanism by which ANS nerve processes facilitate SIV replication in vivo.

The quantitative depletion of catecholaminergic varicosities in SIV-infected lymph nodes suggests that lentiviral pathology might potentially alter the distribution of neural fibers in lymphoid tissue. This finding is independent of the relationship between catecholaminergic varicosities and local SIV replication rates within a given lymph node and suggests a distinct dynamic in which differences in SIV pathogenesis across lymph nodes might influence the overall density of ANS innervation. SIV-induced depletion of lymph node innervation was quantitative, not qualitative, and the majority of SIV-infected tissues still retained parenchymal catecholaminergic varicosities that were associated with localized increases in SIV RNA expression. This quantitative reduction in ANS innervation density is consistent with data from previous studies that showed a depletion of autonomic nerve fibers from the spleens of mice infected with the LP-BM5 mixture of lymphotropic murine

retroviruses (20). The mechanisms by which lymphotropic viruses alter lymphoid tissue innervation are unknown, but at least two broad possibilities exist. One involves neurotoxic effects of viral proteins such as HIV-1 Tat and gp120, which have been shown to induce apoptosis in central nervous system neurons (33) and may cleave the lymphoid chemokine SDF-1 into a neurotoxic by-product (39). A second broad possibility is that cytokines or other signaling molecules released by activated/apoptotic lymphocytes might alter neural architecture. A similar dynamic has been observed in rheumatoid arthritis, where increased expression of semaphorin 3C is associated with a decreased density of catecholaminergic neurons in synovial tissue (24). Regardless of the exact molecular mechanisms involved, the present data suggest that progressing SIV infection may alter autonomic innervation in ways that could potentially affect neuroimmune and neurovirologic interactions. We did not analyze lymph nodes during early-stage acute infection, but the observed depletion of ANS innervation from mid-stage lymphoid tissue with significant viral burden suggests that ANS activation might exert even more pronounced effects on SIV gene expression early in infection, when lymphoid innervation remains dense and viral replication interacts with an emerging immune response to establish the viral load set point. This hypothesis would be consistent with data showing elevated viral load set points in both SIV-infected animals experiencing social stress (5) and HIV-1 patients with high levels of ANS activity (10). Under that scenario, ANS activity early in infection could exert a long-term influence on lentiviral disease progression by altering the dynamic equilibrium between viral replication and antiviral immune responses. Regardless of their potential role in acute viral dynamics, catecholaminergic neural fibers show a strong anatomic relationship to SIV replication within the chronically infected tissues analyzed here. Such relationships are independent of the effect of SIV infection on lymph node cellularity and architecture, and they suggest that ANS activity in lymphoid organs might represent a potential target for adjunctive therapies aimed at limiting long-term physiologic support for lentiviral replication in vivo.

ACKNOWLEDGMENTS

We thank Suzanne Stevens and Srinivasan Thyaga Rajan for help with SPG fluorescence techniques; Harry Vinters and the UCLA AIDS Institute for access to BSL2$^+$ cryostat; Christine Brennan, Erna Tarara, Greg Vicino, Carmel Stanko, Laura Del Rosso, Kristen Cooman, and the Veterinary, Animal Care, and Research Services staff of CNPRC for the conduct of the macaque study; Christina Nguyen for assistance with data analysis; and Jerome Zack and Helen Brown for critically reading the manuscript.

This research was supported by the National Institute of Mental Health (MH049033), the National Institutes of Allergy and Infectious Disease and Neurological Disorders and Stroke (AI/NS052737), the University of California Universitywide AIDS Research Program (CC99-LA-02), the Norman Cousins Center at UCLA, and the James B. Pendelton Charitable Trust.

REFERENCES

1. **Barouch, R., E. Appel, G. Kazimirsky, and C. Brodie.** 2001. Macrophages express neurotrophins and neurotrophin receptors. Regulation of nitric oxide production by NT-3. J. Neuroimmunol. **112:**72–77.
2. **Bellinger, D. L., D. Lorton, C. Lubahn, and D. L. Felten.** 2001. Innervation of lymphoid organs—association of nerves with cells of the immune system and their implications in disease, p. 55–111. *In* R. Ader, D. L. Felten, and N. Cohen (ed.), Psychoneuroimmunology, 3rd ed., vol. 1. Academic Press, San Diego, Calif.
3. **Benschop, R. J., M. Schedlowski, H. Wienecke, R. Jacobs, and R. E. Schmidt.** 1997. Adrenergic control of natural killer cell circulation and adhesion. Brain Behav. Immun. **11:**321–332.
4. **Canto-Nogues, C., S. Jones, R. Sangster, P. Silvera, R. Hull, R. Cook, G. Hall, B. Walker, E. J. Stott, D. Hockley, and N. Almond.** 2001. In situ hybridization and immunolabelling study of the early replication of simian immunodeficiency virus (SIVmacJ5) in vivo. J. Gen. Virol. **82:**2225–2234.
5. **Capitanio, J. P., S. P. Mendoza, N. W. Lerche, and W. A. Mason.** 1998. Social stress results in altered glucocorticoid regulation and shorter survival in simian acquired immune deficiency syndrome. Proc. Natl. Acad. Sci. USA **95:**4714–4719.
6. **Cole, S., and M. E. Kemeny.** 2001. Psychosocial influences on the progression of HIV infection, p. 538–612. *In* R. Ader, D. L. Felten, and N. Cohen (ed.), Psychoneuroimmunology, 3rd ed., vol. 2. Academic Press, San Diego, Calif.
7. **Cole, S. W., B. D. Jamieson, and J. A. Zack.** 1999. cAMP up-regulates cell surface expression of lymphocyte CXCR4: implications for chemotaxis and HIV-1 infection. J. Immunol. **162:**1392–1400.
8. **Cole, S. W., M. E. Kemeny, J. L. Fahey, J. A. Zack, and B. D. Naliboff.** 2003. Psychological risk factors for HIV pathogenesis: mediation by the autonomic nervous system. Biol. Psychiatry **54:**1444–1456.
9. **Cole, S. W., Y. D. Korin, J. L. Fahey, and J. A. Zack.** 1998. Norepinephrine accelerates HIV replication via protein kinase A-dependent effects on cytokine production. J. Immunol. **161:**610–616.
10. **Cole, S. W., B. D. Naliboff, M. E. Kemeny, M. P. Griswold, J. L. Fahey, and J. A. Zack.** 2001. Impaired response to HAART in HIV-infected individuals with high autonomic nervous system activity. Proc. Natl. Acad. Sci. USA **98:**12695–12700.
11. **de la Torre, J. C., and J. W. Surgeon.** 1976. Histochemical fluorescence of tissue and brain monoamines: results in 18 minutes using the sucrose-phosphate-glyoxylic acid (SPG) method. Neuroscience **1:**451–453.
12. **Embretson, J., M. Zupancic, J. L. Ribas, A. Burke, P. Racz, K. Tenner-Racz, and A. T. Haase.** 1993. Massive covert infection of helper T lymphocytes and macrophages by HIV during the incubation period of AIDS. Nature **362:** 359–362.
13. **Felten, D. L., S. Livnat, S. Y. Felten, S. L. Carlson, D. L. Bellinger, and P. Yeh.** 1984. Sympathetic innervation of lymph nodes in mice. Brain Res. Bull. **13:**693–699.
14. **Fleiss, J. L.** 1981. Statistical methods for rates and proportions. Wiley, New York, N.Y.
15. **Guidry, G.** 1999. A method for counterstaining tissues in conjunction with the glyoxylic acid condensation reaction for detection of biogenic amines. J. Histochem. Cytochem. **47:**261–264.
16. **Hill, C. E., J. K. Phillips, and S. L. Sandow.** 1999. Development of peripheral autonomic synapses: neurotransmitter receptors, neuroeffector associations and neural influences. Clin. Exp. Pharmacol. Physiol. **26:**581–590.
17. **Kalinichenko, V. V., M. B. Mokyr, L. H. Graf, Jr., R. L. Cohen, and D. A. Chambers.** 1999. Norepinephrine-mediated inhibition of antitumor cytotoxic T lymphocyte generation involves a beta-adrenergic receptor mechanism and decreased TNF-alpha gene expression. J. Immunol. **163:**2492–2499.
18. **Kammer, G. M.** 1988. The adenylate cyclase-cAMP-protein kinase A pathway and regulation of the immune response. Immunol. Today **9:**222–229.
19. **Kannan, Y., J. Bienenstock, M. Ohta, A. M. Stanisz, and R. H. Stead.** 1996. Nerve growth factor and cytokines mediate lymphoid tissue-induced neurite outgrowth from mouse superior cervical ganglia in vitro. J. Immunol. **157:** 313–320.
20. **Kelley, S. P., J. A. Moynihan, S. Y. Stevens, L. J. Grota, and D. L. Felten.** 2003. Sympathetic nerve destruction in spleen in murine AIDS. Brain Behav. Immun. **17:**94–109.
21. **Kopnisky, K. L., D. M. Stoff, and D. M. Rausch.** 2004. Workshop report: the effects of psychological variables on the progression of HIV-1 disease. Brain Behav. Immun. **18:**246–261.
22. **Leutenegger, C. M., J. Higgins, T. B. Matthews, A. F. Tarantal, P. A. Luciw, N. C. Pedersen, and T. W. North.** 2001. Real-time TaqMan PCR as a specific and more sensitive alternative to the branched-chain DNA assay for quantitation of simian immunodeficiency virus RNA. AIDS Res. Hum. Retrovir. **17:**243–251.
23. **Madden, K. S., V. M. Sanders, and D. L. Felten.** 1995. Catecholamine influences and sympathetic neural modulation of immune responsiveness. Annu. Rev. Pharmacol. Toxicol. **35:**417–448.
24. **Miller, L. E., C. Weidler, W. Falk, P. Angele, J. Schaumburger, J. Scholmerich, and R. H. Straub.** 2004. Increased prevalence of semaphorin 3C, a repellent of sympathetic nerve fibers, in the synovial tissue of patients with rheumatoid arthritis. Arthritis Rheum. **50:**1156–1163.
25. **Miller, R. G.** 1986. Beyond ANOVA. Basics of applied statistics. Wiley, New York, N.Y.
26. **Mouton, P. R.** 2002. Principles and practices of unbiased stereology. An introduction for bioscientists. John Hopkins University Press, Baltimore, Md.
27. **O'Neil, S. P., S. P. Mossman, D. H. Maul, and E. A. Hoover.** 1999. In vivo cell and tissue tropism of SIVsmmPBj14-bcl.3. AIDS Res. Hum. Retrovir. **15:** 203–215.
28. **Orenstein, J. M., M. Feinberg, C. Yoder, L. Schrager, J. M. Mican, D. J.**

Schwartzentruber, R. T. Davey, Jr., R. E. Walker, J. Falloon, J. A. Kovacs, K. D. Miller, C. Fox, J. A. Metcalf, H. Masur, and M. A. Polis. 1999. Lymph node architecture preceding and following 6 months of potent antiviral therapy: follicular hyperplasia persists in parallel with p24 antigen restoration after involution and CD4 cell depletion in an AIDS patient. AIDS **13:**2219–2229.

29. **Ottaway, C. A., and A. J. Husband.** 1994. The influence of neuroendocrine pathways on lymphocyte migration. Immunol. Today **15:**511–517.
30. **Pantaleo, G., C. Graziosi, J. F. Demarest, L. Butini, M. Montroni, C. H. Fox, J. M. Orenstein, D. P. Kotler, and A. S. Fauci.** 1993. HIV infection is active and progressive in lymphoid tissue during the clinically latent stage of disease. Nature **362:**355–358.
31. **Sapolsky, R. M.** 1998. Why zebras don't get ulcers: an updated guide to stress, stress related diseases, and coping. W. H. Freeman & Co., New York, N.Y.
32. **Shimizu, N., T. Hori, and H. Nakane.** 1994. An interleukin-1 beta-induced noradrenaline release in the spleen is mediated by brain corticotropin-releasing factor: an in vivo microdialysis study in conscious rats. Brain Behav. Immun. **8:**14–23.
33. **Singh, I. N., R. J. Goody, C. Dean, N. M. Ahmad, S. E. Lutz, P. E. Knapp, A. Nath, and K. F. Hauser.** 2004. Apoptotic death of striatal neurons induced by human immunodeficiency virus-1 Tat and gp120: differential involvement of caspase-3 and endonuclease G. J. Neurovirol. **10:**141–151.
34. **Stevens-Felten, S. Y., and D. L. Bellinger.** 1997. Noradrenergic and peptidergic innervation of lymphoid organs. Chem. Immunol. **69:**99–131.
35. **Tenner-Racz, K., H. J. Stellbrink, J. van Lunzen, C. Schneider, J. P. Jacobs, B. Raschdorff, G. Grosschupff, R. M. Steinman, and P. Racz.** 1998. The unenlarged lymph nodes of HIV-1-infected, asymptomatic patients with high CD4 T cell counts are sites for virus replication and CD4 T cell proliferation. The impact of highly active antiretroviral therapy. J. Exp. Med. **187:**949–959.
36. **Valitutti, S., M. Dessing, and A. Lanzavecchia.** 1993. Role of cAMP in regulating cytotoxic T lymphocyte adhesion and motility. Eur. J. Immunol. **23:**790–795.
37. **Weihe, E., D. Nohr, S. Michel, S. Muller, H. J. Zentel, T. Fink, and J. Krekel.** 1991. Molecular anatomy of the neuro-immune connection. Int. J. Neurosci. **59:**1–23.
38. **Weiner, H.** 1992. Perturbing the organism: the biology of stressful experience. University of Chicago Press, Chicago, Ill.
39. **Zhang, K., G. A. McQuibban, C. Silva, G. S. Butler, J. B. Johnston, J. Holden, I. Clark-Lewis, C. M. Overall, and C. Power.** 2003. HIV-induced metalloproteinase processing of the chemokine stromal cell derived factor-1 causes neurodegeneration. Nat. Neurosci. **6:**1064–1071.